Dirac Neutrino Masses from the Scoto-Seesaw Mechanism

(e-Print: 2606.20119)

Ranjeet Kumar

Seoul National University of Science and Technology (Seoultech)

With Prof. Sin Kyu Kang and Hemant Kumar Prajapati

12th Workshop on Flavor Symmetries and Consequences in Accelerators and Cosmology
18 August 2026

Table of Contents

- Introduction
- Majorana Scoto-Seesaw
- Dirac Scoto-Seesaw Model
- Neutrino Sector Predictions
- Collider Constraints on Z’
- Singlet Scalar Dark Matter
- Fermionic Dark Matter
- Summary

Neutrino Oscillations

- In the SM, neutrinos are massless.
- Neutrino oscillations suggest that neutrinos must be massive.

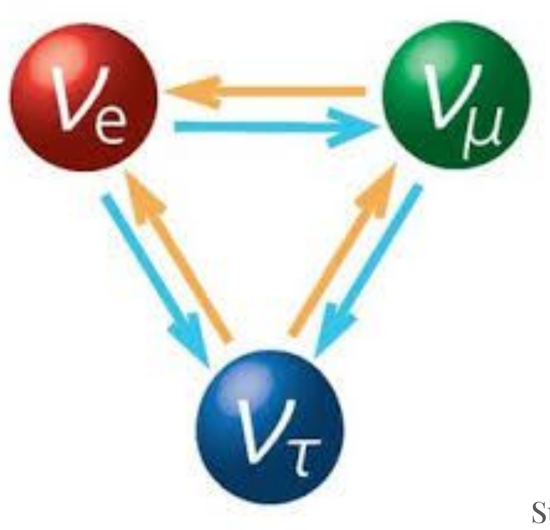

Super-Kamiokande Collaboration. ,
Phys. Rev. Lett. 81 (1998) 1562–1567

Two Mass Squared Differences

- The flavor states of neutrinos, ν_α (α = e, μ, τ), are not mass eigenstates.

- The Mass eigenstates, ν_i (i = 1, 2, 3), are linear combinations of flavor eigenstates.

$$|\nu_i\rangle = \sum_{\alpha=e,\mu,\tau} U_{\alpha i}\, |\nu_\alpha\rangle.$$

- Only two mass squared differences are measured, masses are still unknown. (We also know $m_2 > m_1$).

$$\Delta m^2_{\rm sol} \approx 10^{-5}\ {\rm eV}^2 \qquad \Delta m^2_{\rm atm} \approx 10^{-3}\ {\rm eV}^2$$

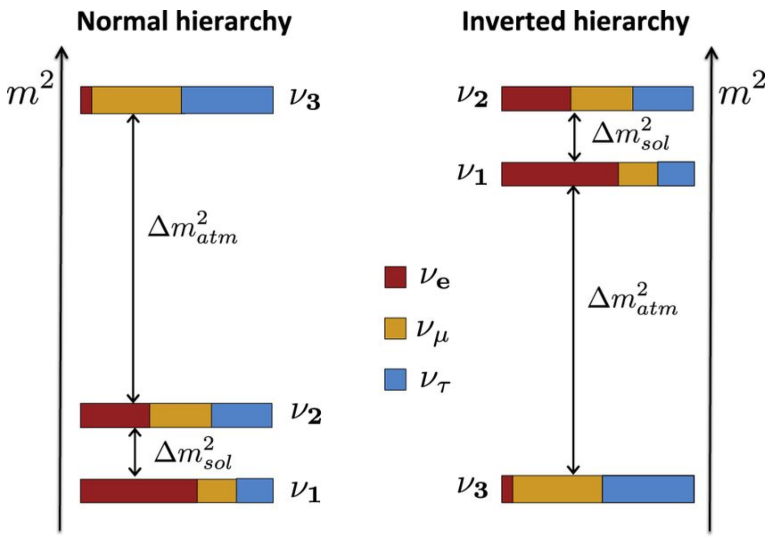

Neutrino mass hierarchy or ordering

Source: Pablo Fernandez.

Super-Kamiokande Collaboration., Phys. Rev. Lett. 81 (1998) 1562–1567, SNO Collaboration., Phys. Rev. Lett. 87 (2001) 071301

Dark Matter Existence

The SM does not contain a viable dark matter candidate.

- Dark matter constitutes ~26.6% of the Universe’s energy density.
- Non-luminous, non-baryonic, and interacts only weakly with ordinary matter.

N. Aghanim et al., 1807.06209

Majorana Scoto-Seesaw Mechanism

- The two distinct neutrino mass scales may originate from two different mechanisms.
- One mass scale arises from the tree-level type-I seesaw, while the other originates from a scotogenic-like loop mechanism.

N. Rojas, R. Srivastava, and J. W. F. Valle,
Phys. Lett. B 789 (2019) 132–136

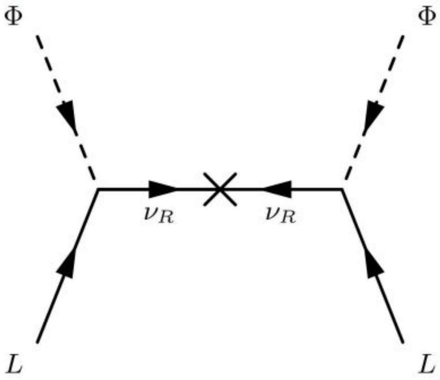

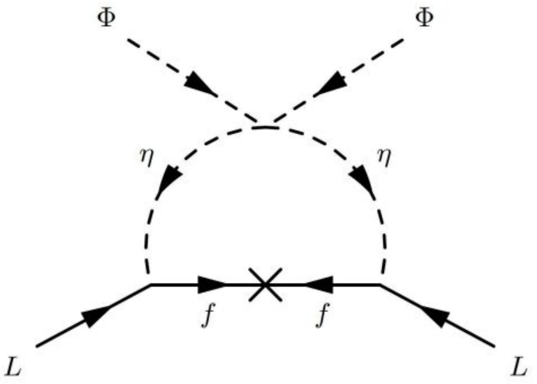

Neutrino mass generation through hybrid scoto-seesaw mechanism. Left: type-I seesaw, right: scotogenic mechanism.

Minkowski 77, Ma, Phys. Rev. D 73 (2006) 077301, D. M. Barreiros, F. R. Joaquim, R. Srivastava, JHEP 04 (2021) 249

The Simplest Dirac Scoto-Seesaw Realization

- We employ a chiral $U(1)_{B\text{-}L}$ symmetry that spontaneously breaks to Z_6.
- This residual Z_6 symmetry forbids Majorana mass terms, ensuring Dirac neutrinos and it also stabilizes the dark matter candidate.

C. Bonilla, et al.,
Phys. Rev. D 101 no. 3, (2020) 033011

	Fields	$SU(2)_L \otimes U(1)_Y$	$U(1)_{B-L} \to \mathbf{Z_6}$
Fermions	L_i	$(2, -1)$	$-1 \to \boldsymbol{\omega^4}$
	e_{R_i}	$(1, -2)$	$-1 \to \boldsymbol{\omega^4}$
	ν_{R_i}	$(1, 0)$	$(-4, -4, 5) \to (\boldsymbol{\omega^4}, \boldsymbol{\omega^4}, \boldsymbol{\omega^4})$
	N_{L_p}, N_{R_p}	$(1, 0)$	$-1 \to \boldsymbol{\omega^4}$
	f_L, f_R	$(1, 0)$	$-1/2 \to \boldsymbol{\omega^5}$
Scalars	H	$(2, 1)$	$0 \to \mathbf{1}$
	χ	$(1, 0)$	$3 \to \mathbf{1}$
	η	$(2, 1)$	$1/2 \to \boldsymbol{\omega}$
	S_1, S_2	$(1, 0)$	$(-11/2, -5/2) \to (\boldsymbol{\omega}, \boldsymbol{\omega})$

TABLE I: Field contents and their transformation properties under $SU(2)_L \otimes U(1)_Y$ and $U(1)_{B-L}$. Here, Z_6 is the residual symmetry, which serves as dark symmetry, and $i = 1, 2, 3$. For case-I (two massive neutrinos) $p = 1$ and for case-II (three massive neutrinos) $p = 2$. Only one generation of f_L, f_R has been introduced.

Dirac Scoto-Seesaw Mechanism

- Neutrino masses and mixing are generated through a hybrid Dirac type-I seesaw and Dirac scotogenic mechanism.

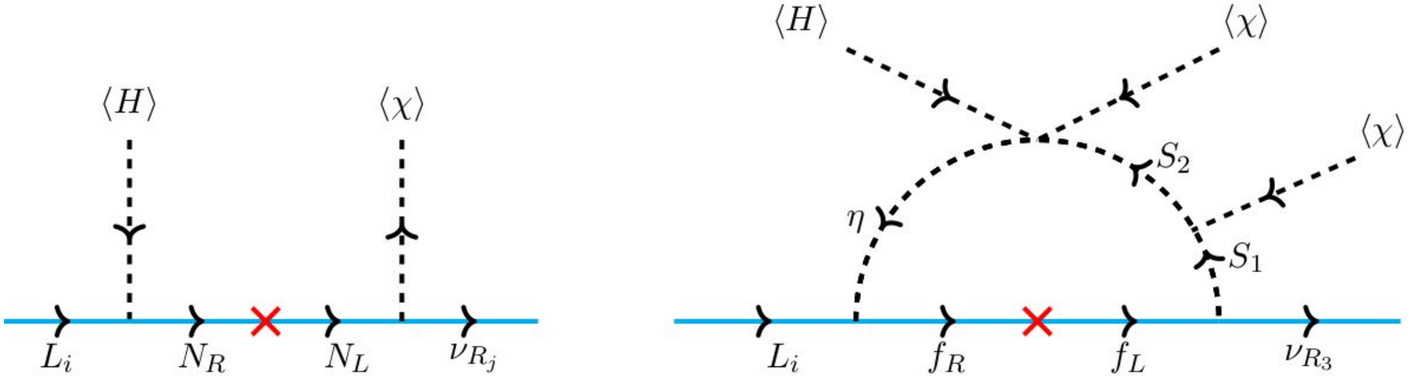

Dirac scoto-seesaw mechanism. Left: Dirac type-I seesaw. Right: Dirac scotogenic mechanism.

Lagrangian and Neutrino Mass Matrix

The Yukawa Lagrangian of the model is given by

$$-\mathcal{L}_Y = Y_e^{ij}\overline{L}_i H e_{R_j} + Y_\nu^{ip}\overline{L}_i \tilde{H} N_{R_p} + M^{qp}\,\overline{N}_{L_q} N_{R_p} + Y_\chi^{q\alpha}\overline{N}_{L_q}\chi \nu_{R_\alpha}$$
$$+ Y_f^i \overline{L}_i \tilde{\eta} f_R + M_f\,\overline{f}_L f_R + y_S\,\overline{f}_L S_1 \nu_{R_3} + \text{H.c.},$$

where, $i, j = 1, 2, 3$, $\alpha = 1, 2$, and $p, q = 1$ $(p, q = 1, 2)$ for case-I (case-II)

The neutrino mass matrices at tree level and loop level can be extracted as

$$\mathcal{M}_\nu = \begin{pmatrix} 0 & \mathcal{M}_\mathcal{D} \\ \mathcal{M}'_\mathcal{D} & \mathcal{M} \end{pmatrix} \Longrightarrow -(m_\nu^{i\alpha})^{(\text{tree})} = \mathcal{M}_\mathcal{D}\mathcal{M}^{-1}\mathcal{M}'_\mathcal{D} = \frac{v_H v_\chi}{2} Y_\nu^{ip}(M^{qp})^{-1} Y_\chi^{q\alpha}$$

$$(m_\nu^i)^{(\text{loop})} = \frac{1}{16\pi^2} Y_f^i y_S \sum_k \mathcal{O}^T[1,k]\mathcal{O}^T[2,k] M_f \left(\frac{M_{\zeta_k}^2}{M_{\zeta_k}^2 - M_f^2}\right) \ln\left(\frac{M_{\zeta_k}^2}{M_f^2}\right) \equiv Y_f^i y_S \mathcal{F}$$

Case-I: Neutrino Mass Observables

- Effective mass of beta decay $|m_\beta| \equiv \sqrt{\sum_i |U_{ei}|^2 m_i^2} = \sqrt{c_{12}^2 c_{13}^2 m_1^2 + s_{12}^2 c_{13}^2 m_2^2 + s_{13}^2 m_3^2}$

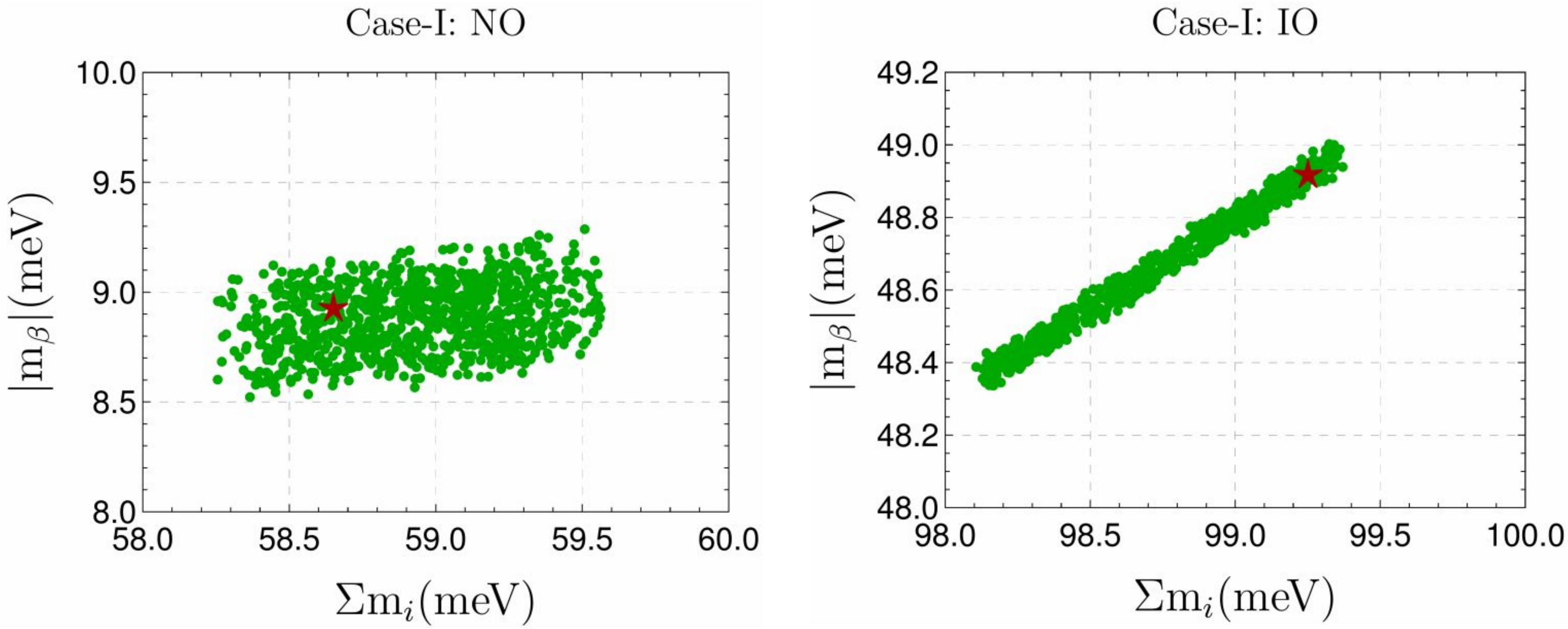

Case-I: CP-violating Phase and Atmospheric Angle

- For NO case: Dirac CP phase close to the CP-conserving value.

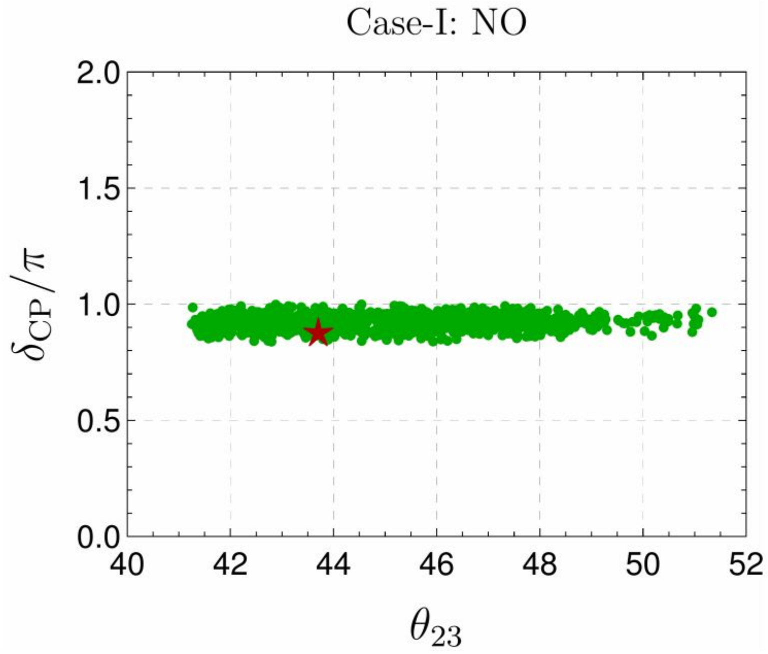

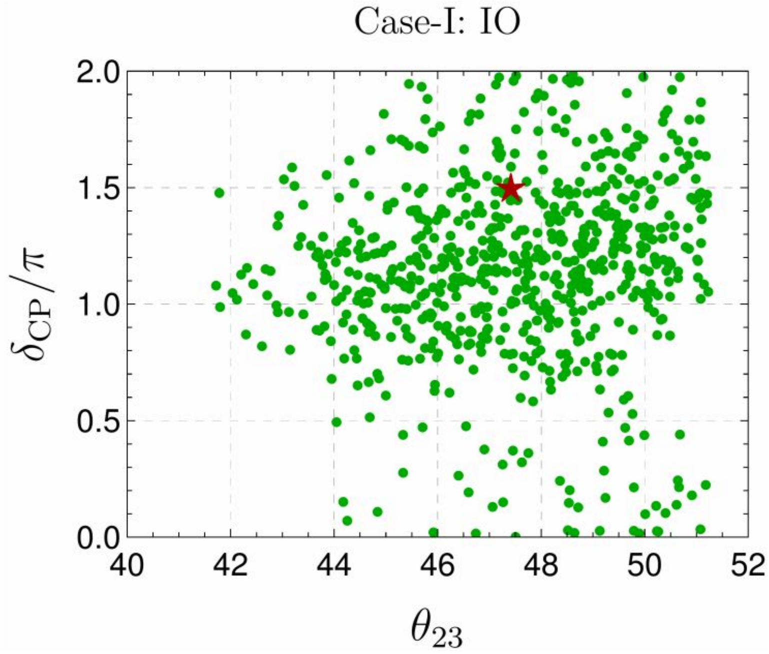

Case-II: Two Mass Squared Differences for IO

- Within the scanned parameter space, the IO scenario cannot simultaneously accommodate both mass squared differences while fitting the neutrino mixing angles.

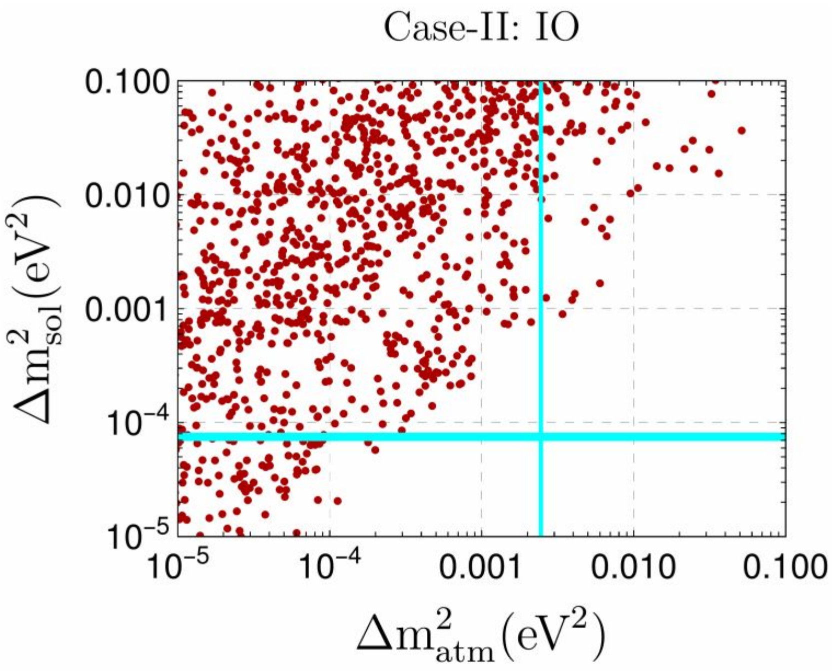

Case-II: Neutrino Mass Observables

- Compared to Case-I, broader ranges are obtained for the effective mass of beta decay and the sum of neutrino masses.

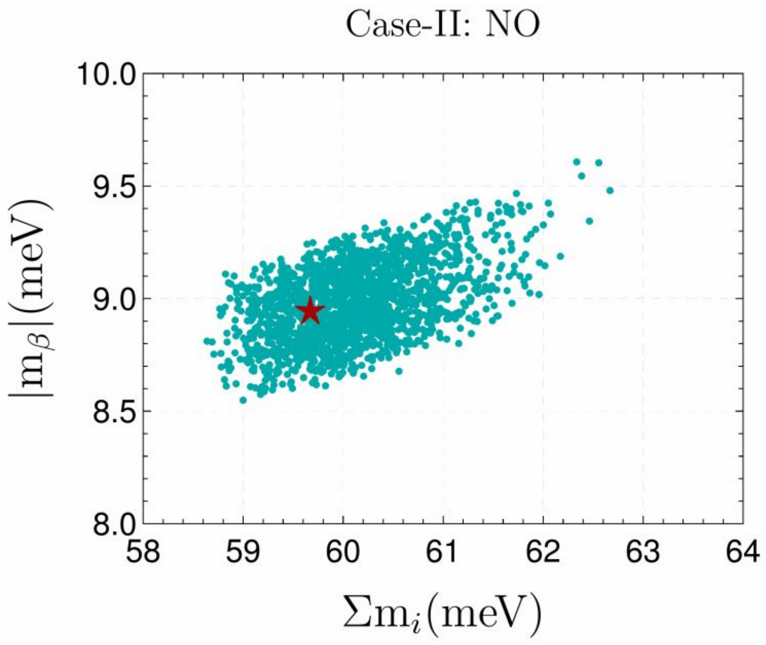

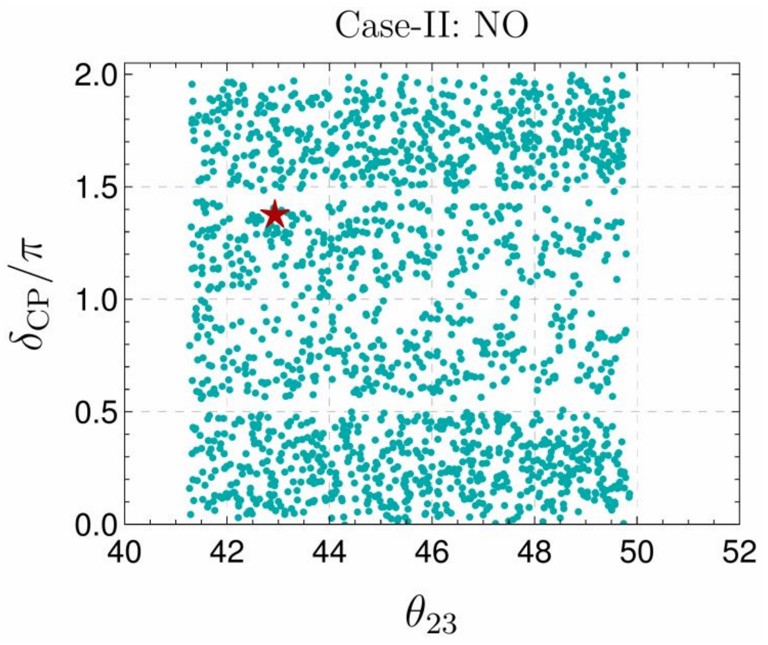

P. F. de Salas, et al., 2006.11237

Collider Constraints on Z' Decay

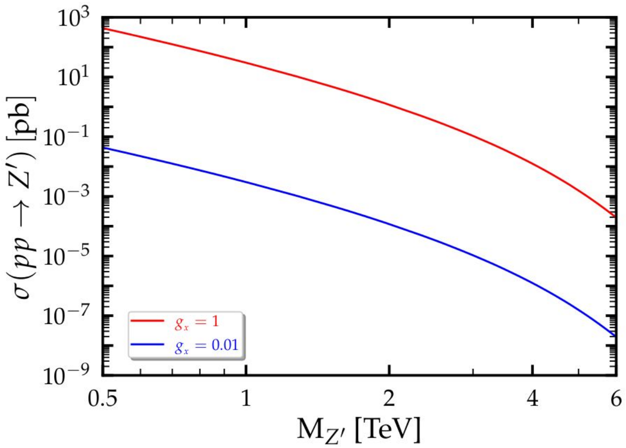

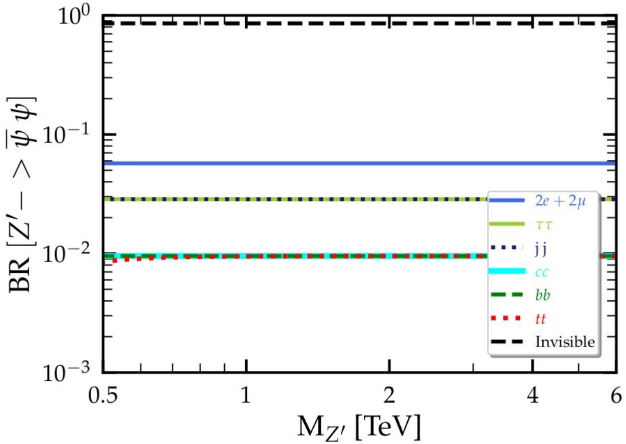

- Production through the Drell–Yan process.
- Decay modes of Z'.
- Constraints on the Z' mass.

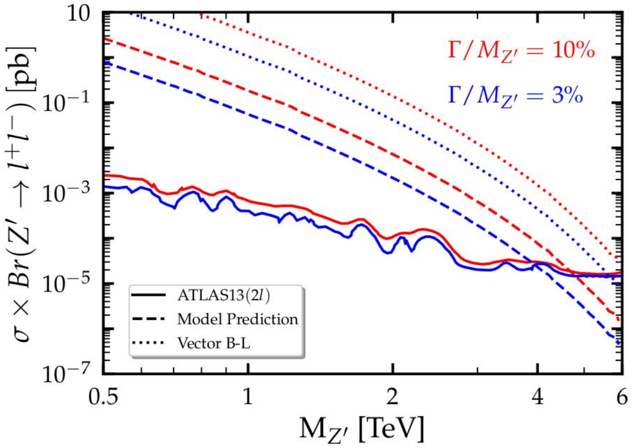

$$\frac{\Gamma(Z' \to \overline{\psi}\psi)}{M_{Z'}} \approx \frac{n_c}{48\pi}\left[(Q_{\psi_L}+Q_{\psi_R})^2 + (Q_{\psi_L}-Q_{\psi_R})^2\right] g_x^2\,,$$

$$\frac{\Gamma}{M_{Z'}} \approx 0.93\, g_x^2.$$

From the chiral B-L, 3.9, 4.6 TeV,
From vector B-L, 5.6, 6 TeV.

Scalar Dark Matter with Z’ Portals

- Considering only the Z' portal for singlet scalar dark matter pushes the viable parameter space close to the current LZ limit.
- Future improvements in direct detection sensitivity could strongly constrain or potentially exclude this scenario.

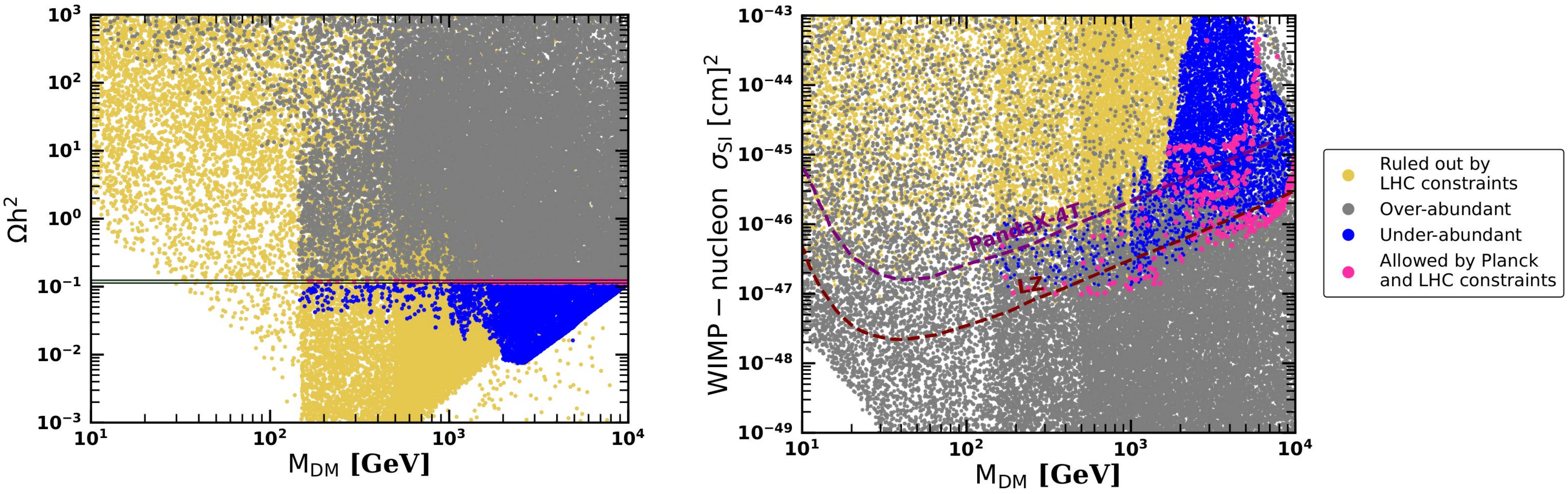

Scalar Dark Matter: S_1- S_2 Mixed Scenario

- Singlet scalar dark matter is strongly constrained by the latest LZ direct detection limits.
- Additional co-annihilation channels in our model open up a broad viable parameter space.

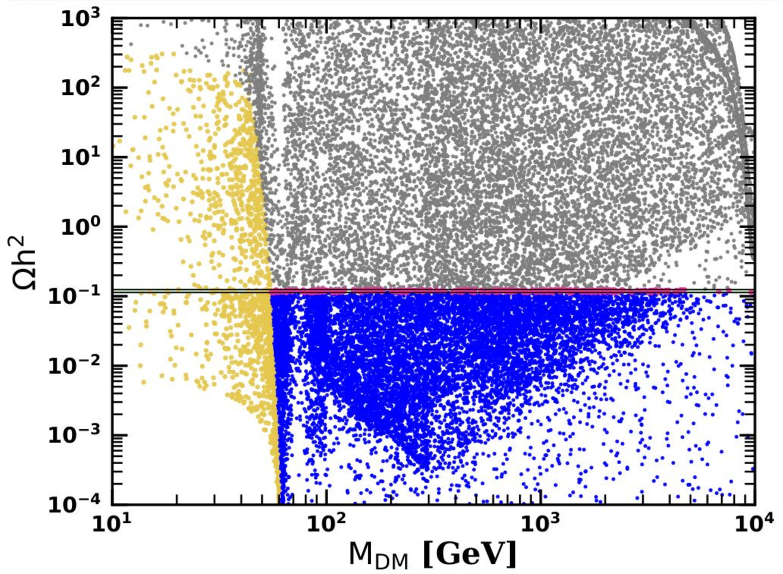

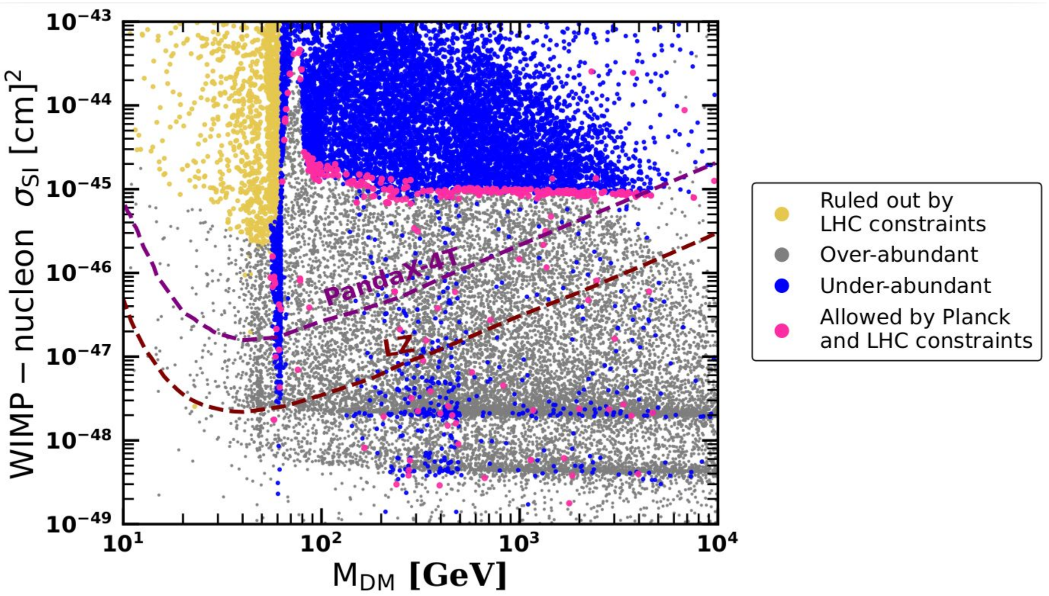

Scalar DM: S_1- S_2 Mixed Scenario with Z' Portals

- Finally, we consider the model predictions including all annihilation and co-annihilation channels, together with the Z' portal interactions.

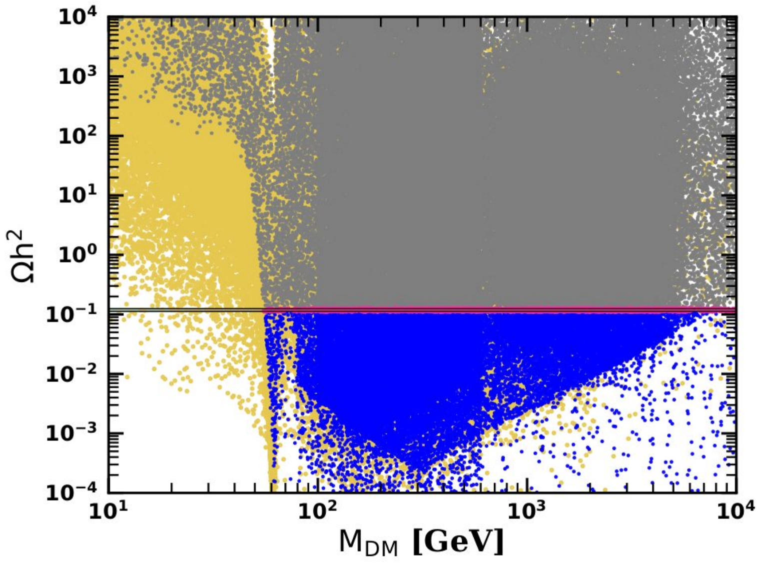

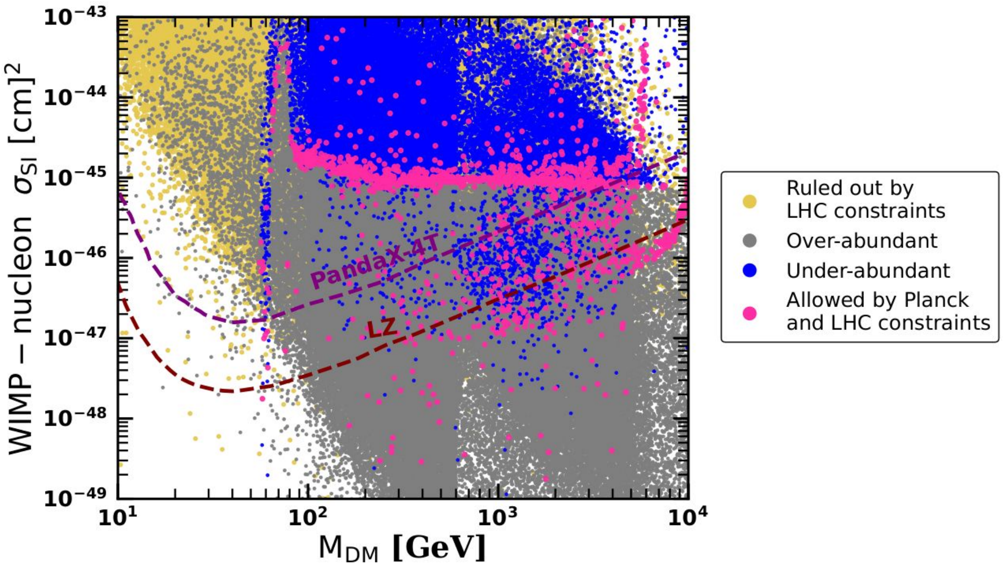

Fermionic Dark Matter

- Fermionic dark matter also remains consistent with current experimental constraints.

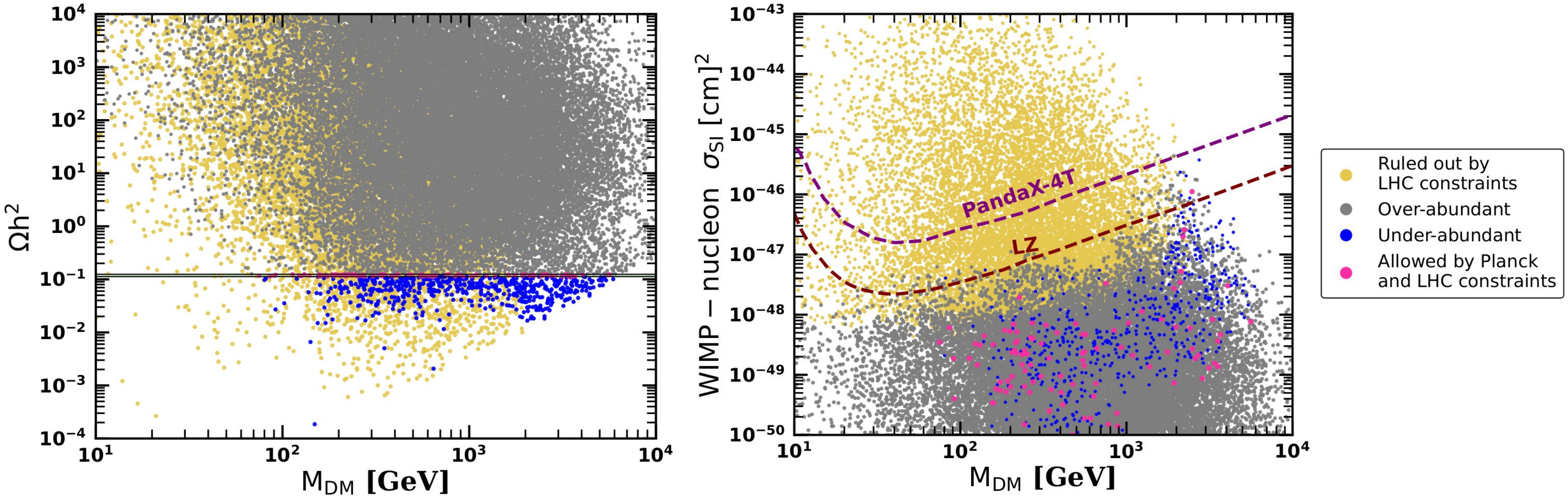

Summary

- The Dirac scoto-seesaw framework simultaneously explains the two observed mass squared differences and provides a viable dark matter candidate.

- The breaking of chiral $U(1)_{B\text{-}L}$ to a residual Z_6 symmetry provides a unified origin for Diracness and dark matter stability.

- Under this chiral $U(1)_{B\text{-}L}$ the limit on Z' mass is weaker than conventional vector B-L.

- Z'-portal and co-annihilation effects open up a broad viable parameter space for singlet scalar dark matter.

- Both scalar and fermionic dark matter scenarios remain compatible with current phenomenological constraints.


Neutrinos
tiny but crucial
Dark Matter
invisible but dominant
Different in nature, connected in the Universe
flavor symmetry
gravitational clue
DM
stability from symmetry
neutrino experiments
Thank You!
direct & indirect detection
Exploring the Unknown, Understanding the Universe

Back Up

...

- We defined chi-square function as $\chi^2 = \sum_i \frac{(x_i - \bar{x}_i)^2}{\sigma_i^2}$,

where $x_i = (\Delta m^2_{31} \text{ or } \Delta m^2_{32}, \Delta m^2_{21}, \sin^2\theta_{12}, \sin^2\theta_{23}, \sin^2\theta_{13})$

Yukawas	Ranges	Masses (in GeV)	Ranges
Y_ν^{i1}	$(10^{-6} - 10^{-2})$	M^{11}	$(10^9 - 10^{10})$
$Y_\chi^{1\alpha}$	$(10^{-6} - 10^{-2})$	M_f	$(10^6 - 10^9)$
Y_f^i, y_S	$\lvert y\rvert e^{i\phi}$	M_{ζ_i}	$(10^1 - 10^5)$

TABLE II: Ranges of the input parameters used for the numerical scan for case-I, where $i = 1, 2, 3$, $\alpha = 1, 2$ and $|y| = (10^{-6} - 10^{-4})$, $\phi \in [0, 2\pi)$. The singlet VEV $v_\chi \approx (10^2 - 10^7)$ GeV.

...

Yukawas	Ranges	Masses (in GeV)	Ranges
$Y_\nu^{i\alpha}$	$(10^{-7} - 10^{-3})$	$M^{\alpha\beta}$	$(10^{10} - 10^{12})$
$Y_\chi^{\alpha\beta}$	$(10^{-7} - 10^{-3})$	M_f	$(10^{5} - 10^{6})$
Y_f^i, y_S	$\lvert y\rvert e^{i\phi}$	M_{ζ_i}	$(10^{1} - 10^{5})$

TABLE V: Ranges of the input parameters used for the numerical scan for case-II, where $i = 1, 2, 3$, $\alpha, \beta = 1, 2$ and $|y| = (10^{-6} - 10^{-4})$, $\phi \in [0, 2\pi)$. The singlet VEV $v_\chi \approx (10^2 - 10^7)$ GeV.

...

Parameters	BF ($\times 10^{-4}$)	Parameters	BF	Observables	BF
Y_ν^{11}	1.07	$Y_f^1(\times 10^{-6})$	$-9.29 - 9.69i$	$\boldsymbol{\theta_{12}}$	**33.96°**
Y_ν^{21}	2.68	$Y_f^2(\times 10^{-5})$	$5.20 + 1.93i$	$\boldsymbol{\theta_{13}}$	**8.68°**
Y_ν^{31}	0.016	$Y_f^3(\times 10^{-5})$	$-3.05 - 5.19i$	$\boldsymbol{\theta_{23}}$	**43.70°**
Y_χ^{11}	6.98	$Y_S(\times 10^{-4})$	$2.58 - 7.5i$	$\boldsymbol{\delta_{CP}}$	$\boldsymbol{0.88\pi}$
Y_χ^{12}	0.014	M^{11} (in GeV)	1.98×10^9	$\boldsymbol{\Delta m^2_{sol}}$ (in eV^2)	$\boldsymbol{7.47 \times 10^{-5}}$
v_χ (in GeV)	8.49×10^5	$\mathcal{F}$ (in GeV)	7.53×10^{-4}	$\boldsymbol{\Delta m^2_{atm}}$ (in eV^2)	$\boldsymbol{2.50 \times 10^{-3}}$
–	–	–	–	$\boldsymbol{\sum m_i}$ (in meV)	**58.65**
–	–	–	–	$\boldsymbol{\vert m_\beta \vert}$ (in meV)	**8.93**

TABLE III: The obtained BF values of input parameters and observables for the NO scenario corresponding to $\chi^2_{\rm min} = 1.475$ for case-I.

Parameters	BF ($\times 10^{-4}$)	Parameters	BF	Observables	BF
Y_ν^{11}	5.18	$Y_f^1(\times 10^{-6})$	$3.61 + 5.62i$	$\boldsymbol{\theta_{12}}$	**33.83°**
Y_ν^{21}	0.55	$Y_f^2(\times 10^{-5})$	$2.60 - 3.01i$	$\boldsymbol{\theta_{13}}$	**8.64°**
Y_ν^{31}	0.79	$Y_f^3(\times 10^{-5})$	$-4.13 - 1.11i$	$\boldsymbol{\theta_{23}}$	**47.41°**
Y_χ^{11}	15.56	$Y_S(\times 10^{-5})$	$-0.49 + 1.23i$	$\boldsymbol{\delta_{CP}}$	$\boldsymbol{1.5\pi}$
Y_χ^{12}	5.65	M^{11} (in GeV)	1.90×10^9	$\boldsymbol{\Delta m^2_{sol}}$ (in eV^2)	$\boldsymbol{7.48 \times 10^{-5}}$
v_χ (in GeV)	8.73×10^5	$\mathcal{F}$ (in GeV)	6.38×10^{-2}	$\boldsymbol{\Delta m^2_{atm}}$ (in eV^2)	$\boldsymbol{2.42 \times 10^{-3}}$
–	–	–	–	$\boldsymbol{\sum m_i}$ (in meV)	**99.25**
–	–	–	–	$\boldsymbol{\vert m_\beta \vert}$ (in meV)	**48.92**

TABLE IV: Best fit values of input parameters and observables for the IO scenario corresponding to $\chi^2_{\rm min} = 9.033$ for case-I.

…

Parameters	BF ($\times 10^{-5}$)	Parameters	BF	Observables	BF
Y_ν^{11}, Y_ν^{22}	3.70	$Y_f^1 (\times 10^{-6})$	$-0.095 - 2.18i$	$\boldsymbol{\theta_{12}}$	$\mathbf{33.91^\circ}$
Y_ν^{12}	2.20	$Y_f^2 (\times 10^{-6})$	$-9.03 + 3.07i$	$\boldsymbol{\theta_{13}}$	$\mathbf{8.62^\circ}$
Y_ν^{21}	0.025	$Y_f^3 (\times 10^{-6})$	$9.99 - 3.25i$	$\boldsymbol{\theta_{23}}$	$\mathbf{42.93^\circ}$
Y_ν^{31}	0.17	$Y_S (\times 10^{-6})$	$-22.14 - 1.04i$	$\boldsymbol{\delta_{CP}}$	$\mathbf{1.38\pi}$
Y_ν^{32}	7.9	M^{11} (in GeV)	3.84×10^{11}	$\boldsymbol{\Delta m^2_{sol}}$ (in eV^2)	$\mathbf{7.58 \times 10^{-5}}$
Y_χ^{11}, Y_χ^{22}	41.00	M^{22} (in GeV)	5.76×10^{10}	$\boldsymbol{\Delta m^2_{atm}}$ (in eV^2)	$\mathbf{2.51 \times 10^{-3}}$
Y_χ^{12}	0.67	$\mathcal{F}$ (in GeV)	-0.157	$\boldsymbol{\sum_i m_i}$ (in meV)	**59.67**
Y_χ^{21}	1.20	v_χ (in GeV)	2.06×10^5	$\boldsymbol{\lvert m_\beta \rvert}$ (in meV)	**8.95**

TABLE VI: Best fit values of input parameters and observables for the NO scenario corresponding to $\chi^2_{\rm min} = 0.536$ for case-II.

…

$$
\begin{aligned}
\mathcal{V}_{\mathrm{S}} = {} & m_H^2 H^\dagger H + \frac{\lambda_1}{2}(H^\dagger H)^2 + m_\eta^2 \eta^\dagger \eta + \frac{\lambda_2}{2}(\eta^\dagger \eta)^2 + \lambda_3 (H^\dagger H)(\eta^\dagger \eta) + \lambda_4 (H^\dagger \eta)(\eta^\dagger H) \\
& + m_\chi^2 (\chi^* \chi) + \frac{\lambda_\chi}{2}(\chi^* \chi)^2 + m_{s_i}^2 (S_i^* S_i) + \frac{\lambda_{s_i}}{2}(S_i^* S_i)^2 + \lambda_{H\chi}(H^\dagger H)(\chi^* \chi) + \lambda_{\eta\chi}(\eta^\dagger \eta)(\chi^* \chi) \\
& + \lambda_{Hs_i}(H^\dagger H)(S_i^* S_i) + \lambda_{\eta s_i}(\eta^\dagger \eta)(S_i^* S_i) + \lambda_{\chi s_i}(\chi^* \chi)(S_i^* S_i) + \lambda_{s_1 s_2}(S_1^* S_1)(S_2^* S_2) \\
& + (\lambda_6 H^\dagger \eta \chi^* S_2^* + \kappa S_2 \chi^* S_1^* + \mathrm{H.c.})\,.
\end{aligned}
$$

$$
\mathcal{M}_{\mathrm{DM}}^2 = \begin{pmatrix}
m_\eta^2 + \frac{v_H^2}{2}(\lambda_3 + \lambda_4) + \lambda_{\eta\chi}\frac{v_\chi^2}{2} & 0 & \frac{v_H v_\chi}{2}\lambda_6 \\
0 & m_{s_1}^2 + \frac{1}{2}(\lambda_{Hs_1} v_H^2 + \lambda_{\chi s_1} v_\chi^2) & \kappa \frac{v_\chi}{\sqrt{2}} \\
\frac{v_H v_\chi}{2}\lambda_6 & \kappa \frac{v_\chi}{\sqrt{2}} & m_{s_2}^2 + \frac{1}{2}(\lambda_{Hs_2} v_H^2 + \lambda_{\chi s_2} v_\chi^2)
\end{pmatrix}
$$

This mass matrix is rotated to the mass basis by an orthogonal matrix $\mathcal{O}$. The mass eigenstates ζ_p and the gauge eigenstates $H^D = (\eta_0, S_1, S_2)$ are related as $\zeta_p = \mathcal{O}[p,q] H_q^D$, with $p, q = 1, 2, 3$.

$$
M_Z^2 = \frac{v_H^2}{4}(g^2 + g'^2),\ M_W^2 = \frac{v_H^2 g^2}{4},\ M_{Z'} = 3 v_\chi g_x
$$

…

Source: Taken from FLASY 2026 talk of J. W. F. Valle.